Contents lists available at ScienceDirect

# Brain Research Bulletin

journal homepage: www.elsevier.com/locate/brainresbull





# Disease-specific resting-state EEG network variations in schizophrenia revealed by the contrastive machine learning

Fali Li  $^{a,b,c,d}$ , Guangying Wang  $^{a,b}$ , Lin Jiang  $^{a,b}$ , Dezhong Yao  $^{a,b,d,e}$ , Peng Xu  $^{a,b,d,f,g,*}$ , Xuntai Ma  $^{h,i,**}$ , Debo Dong  $^{j,k,***}$ , Baoming He  $^{l,m,****}$ 

- a The Clinical Hospital of Chengdu Brain Science Institute, MOE Key Lab for Neuroinformation, University of Electronic Science and Technology of China, Chengdu 611731, China
- School of Life Science and Technology, Center for Information in BioMedicine, University of Electronic Science and Technology of China, Chengdu 611731, China
- <sup>c</sup> Department of Electrical and Computer Engineering, Faculty of Science and Technology, University of Macau, Macau, China
- d Research Unit of NeuroInformation, Chinese Academy of Medical Sciences, 2019RU035 Chengdu, China
- School of Electrical Engineering, Zhengzhou University, Zhengzhou 450001, China
- <sup>f</sup> Radiation Oncology Key Laboratory of Sichuan Province, Chengdu 610041, China
- g Rehabilitation Center, Qilu Hospital of Shandong University, Jinan 250012, China
- <sup>h</sup> Clinical Medical College of Chengdu Medical College, Chengdu 610500, China
- <sup>i</sup> The First Affiliated Hospital of Chengdu Medical College, Chengdu 610599, China
- <sup>j</sup> Faculty of Psychology, Southwest University, Chongqing 400715, China
- k Institute of Neuroscience and Medicine, Brain and Behavior (INM-7), Research Center Jülich, Jülich, Germany
- <sup>1</sup> Department of Neurology, Sichuan Provincial People's Hospital, University of Electronic Science and Technology of China, Chengdu 610072, China
- m Chinese Academy of Sciences Sichuan Translational Medicine Research Hospital, Chengdu 610072, China

#### ARTICLE INFO

#### Keywords: Schizophrenia Contrastive variational autoencoders Disease-specific network patterns Network disconnectivity

#### ABSTRACT

Given a multitude of genetic and environmental factors, when investigating the variability in schizophrenia (SCZ) and the first-degree relatives (R-SCZ), latent disease-specific variation is usually hidden. To reliably investigate the mechanism underlying the brain deficits from the aspect of functional networks, we newly iterated a framework of contrastive variational autoencoders (cVAEs) applied in the contrasts among three groups, to disentangle the latent resting-state network patterns specified for the SCZ and R-SCZ. We demonstrated that the comparison in reconstructed resting-state networks among SCZ, R-SCZ, and healthy controls (HC) revealed network distortions of the inner-frontal hypoconnectivity and frontal-occipital hyperconnectivity, while the original ones illustrated no differences. And only the classification by adopting the reconstructed network metrics achieved satisfying performances, as the highest accuracy of 96.80%  $\pm$  2.87%, along with the precision of 95.05%  $\pm$  4.28%, recall of 98.18%  $\pm$  3.83%, and F1-score of 96.51%  $\pm$  2.83%, was obtained. These findings consistently verified the validity of the newly proposed framework for the contrasts among the three groups and provided related resting-state network evidence for illustrating the pathological mechanism underlying the brain deficits in SCZ, as well as facilitating the diagnosis of SCZ.

## 1. Introduction

As a widely accepted lifetime neuropsychiatric syndrome, schizophrenia (SCZ) is usually characterized by multiple symptoms and signs of unknown etiology and has been linked to cognitive disturbances in recognizing, processing, and responding to novel stimuli (Insel, 2010; Murillo-Garcia et al., 2022). Compared to the healthy populations, previous studies have greatly revealed deficits in multiple brain regions

E-mail addresses: xupeng@uestc.edu.cn (P. Xu), maxuntai2002@126.com (X. Ma), debodong@swu.edu.cn (D. Dong), hbmneuro@163.com (B. He).

https://doi.org/10.1016/j.brainresbull.2023.110744

Received 27 June 2023; Received in revised form 3 August 2023; Accepted 14 August 2023 Available online 15 August 2023

0361-9230/© 2023 The Author(s). Published by Elsevier Inc. This is an open access article under the CC BY-NC-ND license (http://creativecommons.org/licenses/bync-nd/4.0/).

<sup>\*</sup> Corresponding author at: The Clinical Hospital of Chengdu Brain Science Institute, MOE Key Lab for Neuroinformation, University of Electronic Science and Technology of China, Chengdu 611731, China.

<sup>\*\*</sup> Corresponding author at: Clinical Medical College of Chengdu Medical College, Chengdu 610500, China.

<sup>\*\*\*</sup> Corresponding author at: Faculty of Psychology, Southwest University, Chongqing 400715, China.

<sup>\*\*\*\*</sup> Corresponding author at: Department of Neurology, Sichuan Provincial People's Hospital, University of Electronic Science and Technology of China, Chengdu 610072, China.

of SCZ patients, such as the anterior cingulate cortex and prefrontal cortex (Li et al., 2018; Mouchlianitis et al., 2015), as well as their inter-regional communications, which is commonly termed as "disconnectivity hypothesis" (Stephan et al., 2009).

As illustrated previously, the resting-state activity consumes the majority of the brain energy (exceeding 95%) (Raichle, 2010), thus spontaneous activity is believed to reflect the potential of the brain to efficiently process information (Jiang et al., 2023b; Si et al., 2023; Zhang et al., 2016), as well as offer abundant accounts for elaborating the illness-induced distortions (Feng et al., 2023; Yang et al., 2023). Particularly, multiple spatially distributed but functionally linked regions (Li et al., 2023; Yi et al., 2022) in the brain coupled with each other, forming a larger-scale complex network (Bassett and Sporns, 2017; Jiang et al., 2023a; Sporns, 2022). Concerning the resting-state networks, over the past decades, plenty of resting-state studies have provided a bulk of evidence for explaining the intrinsic brain abnormalities in SCZ (da Cruz et al., 2020; Jiang et al., 2022; Li et al., 2022; Yang et al., 2015). For example, when exploring the distortions in functional subsystems in SCZ, both decreased executive control and dorsal attention networks and the attenuated integration between the executive control and default mode networks were identified (Woodward et al., 2011).

However, from a macroscopic perspective, the human brain is shaped by a multitude of genetic and environmental factors, the diseasespecific variations are thus difficult to be identified, due to the mass of multiple irrelevant factors. On one hand, neurophysiological biomarkers of psychosis risk have been previously investigated, which aims to explain how related pathological risk is conferred (Wang et al., 2022). And a portion of the identified biomarkers has been indeed reported to be closely associated with increased psychosis risk, as well as help predict its transition (Lepock et al., 2018). For example, significant volume reductions in left anterior cornu ammonis were found for the relatives, which deviated from the healthy controls (HC), while a significantly larger right posterior subiculum was reported when compared with first-episode SCZ (Choi et al., 2022). In addition, it has also been clinically proven that SCZ and their first-degree relatives (R-SCZ) carry similar disease-specific genes (Sullivan et al., 2003), and previous studies had further reported a continuous increase of the genetic SCZ risk variation burden from unaffected family members to SCZ patients (Ahangari et al., 2022). However, in related studies, apart from some obvious variations uncovered and reported, in most cases, it is difficult for us to clearly depict the variability existing between patients and their relatives. Hence, recent studies have proposed a framework defining the contrastive variational autoencoders (cVAEs) to disentangle autism-specific neuroanatomical variation from typical developing participants (Aglinskas et al., 2022). In this work, they successfully extracted the autism-specific variation and reported close associations between autism-specific variation and individual symptoms. Herein, we mainly tried to disentangle the disease-specific variations from the shared background across the SCZ, R-SCZ, and HC, to uncover the patient- and relative-specific restings-state network structures.

Overall, SCZ has been widely clarified to be attributed to brain network disconnectivity (Jiang et al., 2022; Stephan et al., 2009), and related neurophysiological markers, also referring as endophenotypes, have been reported to be impaired in the R-SCZ (Wang et al., 2022), as well, which can help decode how related genetic risk is conferred. Herein, given that recent studies cannot always efficiently capture the disease-specific variations among varying populations, we thus concentrated on this latent issue and attempted to disentangle the latent disease-specific network disconnectivity from what is common among the three groups. And further, a promoted aim of our current study was to resolve if the reconstructed networks could provide new evidence elaborating the network distortions in SCZ, as well as provide possible biomarkers for the clinical diagnosis of SCZ. Therefore, based on the originally constructed resting-state electroencephalogram (EEG) networks of all participants, a new framework of cVAEs was iterated to

accomplish the decomposition of functional networks among the three groups. In the meantime, the resting-state activity has been widely acknowledged to provide possible biomarkers for recognizing SCZ (Li et al., 2022; Li et al., 2019; Nunez et al., 2017), for instance, a high accuracy of approximately 90% was achieved using two rest EEG network measurements to classify amnestic mild cognitive impairment from normal cognition (Xu et al., 2014b). Herein, we would further reveal whether these network variations disentangled could help facilitate the diagnosis of SCZ.

#### 2. Results

Herein, we primarily concentrated on the resting-state networks to explore the disease-specific deficits in the brain of SCZ. For all participants, after data preprocessing, the PLV networks were first constructed and accordingly compared among the three groups, however, no differences were reported (p>0.05, Bonferroni corrected). Hence, to further capture the differences in resting-state networks among these groups, by inputting the original networks into the cVAEs, the latent patient- and relative-specific network variations were disentangled, which was similar to the concept of contrastive principal component analysis. Thereafter, for all participants, the characteristic matrices were extracted, accordingly reconstructing the resting-state networks. Fig. 1 reports the comparison between original and reconstructed resting-state networks, illustrating no significant differences (p>0.05, Bonferroni corrected), which confirmed the reliability of the network reconstruction.

Given the original networks failed in mining between-group differences (HC vs. R-SCZ, HC vs. SCZ, and R-SCZ vs. SCZ), we then tried if the reconstructed networks could work. Concretely, based on the reconstructed networks, topological differences among the three groups were explored, which did capture potential variability across groups. Just as displayed in Fig. 2 (p < 0.05, Bonferroni corrected), when comparing both SCZ and R-SCZ with HC, we consistently found decreased shortrange inner-frontal connectivity, as well as increased long-range frontal-occipital connectivity for both groups. And when comparing the R-SCZ and SCZ, both weaker bilateral temporal connectivity and stronger long-rang frontal-parietal connectivity were uncovered for SCZ. Concerning the resting-state network properties, for both original and reconstructed networks, four network properties, e.g., clustering coefficients (CC), characteristic path length (CPL), global efficiency (GE), and local efficiency (LE), showed no significant differences among the three groups (p > 0.05, Bonferroni corrected).

In recent decades, achieving the accurate recognition of SCZ always draws huge attention. Our following analyses then tried if the original and reconstructed networks could help facilitate the classification of SCZ. On one hand, based on the original networks, both the network topologies and properties were applied to accomplish the classification, and as listed in Table 1, we only acquired an accuracy of 31.56%  $\pm$  7.51% for network properties and of 35.38%  $\pm$  9.14% for network topologies, which was obviously lower than expected. On the other hand, both topologies and properties of the reconstructed networks were used, as well. In Table 1, we did find that when reconstructed network topologies were used, the highest accuracy of 96.80%  $\pm$  2.87% was acquired, along with the precision of 95.05%  $\pm$  4.28%, recall of 98.18%  $\pm$  3.83%, and F1-score of 96.51%  $\pm$  2.83%. Whereas, the network properties still acquired unsatisfying performance, only an accuracy of 34.75%  $\pm$  6.30% was obtained.

Apart from the classification among these three groups, we further validated if the reconstructed network topologies could also succeed in recognizing SCZ from their relatives. Thus, following a similar cross-validation strategy, the classification of SCZ vs. R-SCZ was accomplished. Herein, we acquired an accuracy of 91.40%  $\pm$  9.63%, as well as a precision of 92.86%  $\pm$  7.09%, recall of 92.29%  $\pm$  8.28%, and F1-score of 91.16%  $\pm$  9.80%, which did clarify the validity of the reconstructed network topologies in facilitating the recognition of SCZ.

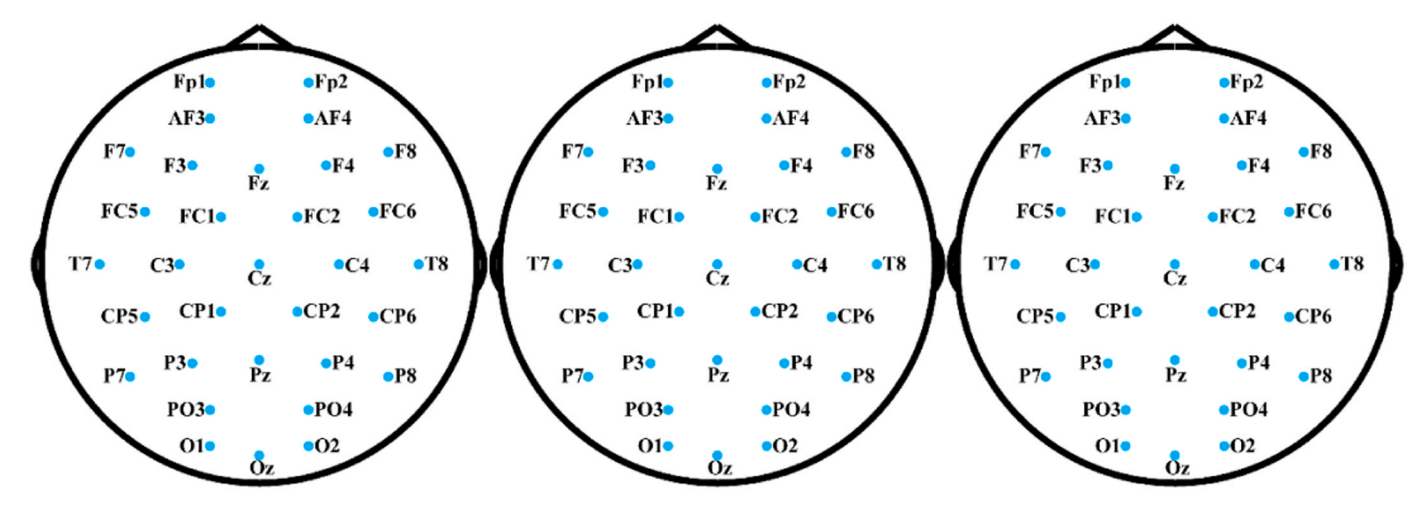


Fig. 1. Statistics between the original and reconstructed resting-state networks based on the cVAEs for the HC, R-SCZ, and SCZ groups (p > 0.05, Bonferroni corrected), respectively.

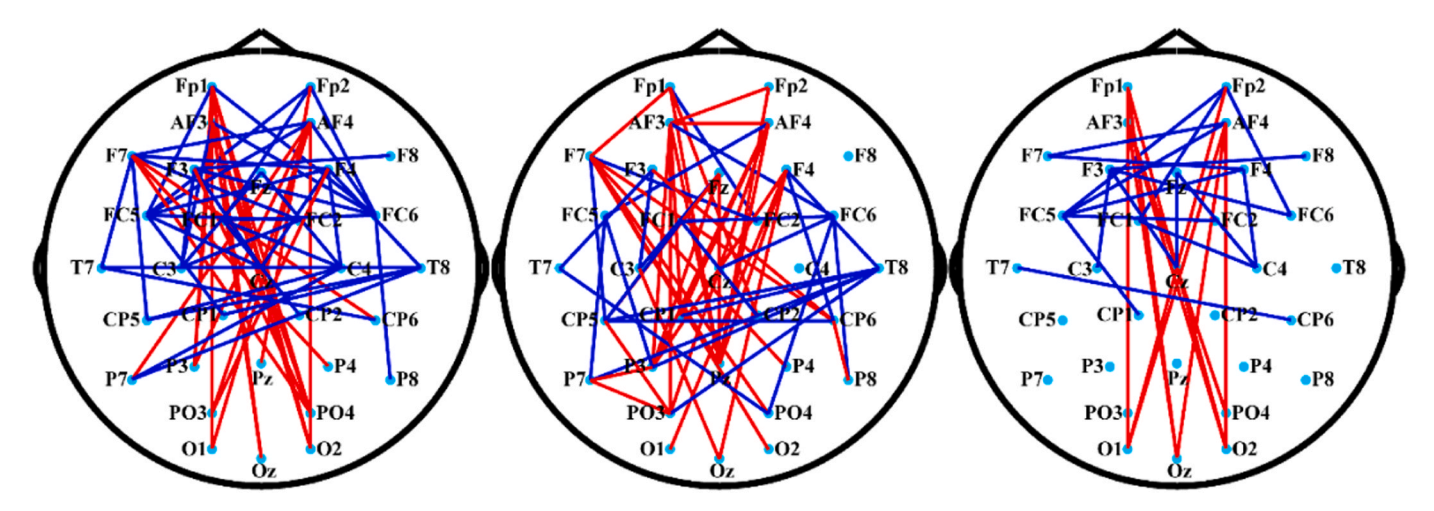


Fig. 2. Comparison of the reconstructed resting-state networks among the three groups. In each subfigure, the blue-solid lines denote the stronger edges in variable 1 (HC, R-SCZ, and HC, respectively) than that in variable 2 (SCZ, SCZ, and R-SCZ, respectively), while the red-solid lines denote the opposite.

 Table 1

 Classification performances based on the resting-state network metrics.

	Original resti	ng-state networks	Reconstructed resting-state networks	
	Properties	Topologies	Properties	Topologies
Accuracy	31.56%	35.38%	34.75%	96.80%
	$\pm\ 7.51\%$	$\pm$ 9.14%	$\pm$ 6.30%	$\pm$ 2.87%
Precision	14.02%	41.56%	11.58%	95.05%
	$\pm~8.15\%$	$\pm~10.16\%$	$\pm~2.10\%$	$\pm$ 4.28%
Recall	33.07%	5015%	33.33%	98.18%
	$\pm$ 2.31%	$\pm$ 19.73%	$\pm~0.01\%$	$\pm$ 3.83%
F1-score	17.18%	44.66%	17.08%	96.51%
	$\pm \ 4.95\%$	$\pm\ 13.95\%$	$\pm\ 2.37\%$	$\pm~2.83\%$

Moreover, given deficits in P300 amplitudes are regarded as an endophenotype of SCZ (Chun et al., 2013; Jeon and Polich, 2003), it has been widely applied to discriminate SCZ from HC (Li et al., 2019; Turetsky et al., 2015). Hence, the P300 amplitudes were also considered in achieving the classification of SCZ. In this study, considering not all participants had both resting-state and task designs, we thus only brought participants who had both resting-state and task EEG datasets into the subsequent analyses, which consisted of 74 HCs, 69 SCZs, and 94 R-SCZs. Thereafter, for these participants, based on their

trial-averaged ERP signals, the P300 amplitudes were extracted within a time duration of [300, 500] ms (0 ms denotes the target onsets). And we statistically investigated the potential differences in P300 amplitudes. Just as displayed in Fig. 3, the P300 amplitudes of SCZ were the smallest (vs. R-SCZ: t=-2.11, p=0.04; vs. HC: t=-4.51, p<0.00), and the R-SCZ also showed the smaller P300 amplitudes (t=-2.52, t=0.01), when compared to that of HC.

Eventually, the P300 amplitudes were regarded as discriminative features to accomplish the classification. The results showed that the P300 amplitudes only acquired an accuracy of  $38.86\% \pm 9.31\%$ , precision of  $20.76\% \pm 13.03\%$ , recall of  $36.65\% \pm 4.06\%$ , and F1-score of  $23.87\% \pm 10.08\%$ , which is still lower than expected. On the contrary, the network topologies still acquired the highest accuracy of  $94.93\% \pm 4.82\%$ , along with a precision of  $95.28\% \pm 8.05\%$ , recall of  $93.81\% \pm 11.24\%$ , and F1-score of  $93.88\% \pm 6.57\%$ . These consistently validated again that the reconstructed resting-state network topologies were helpful and would provide potential biomarkers for the diagnosis of SCZ. Table 2.

# 3. Discussion

As proven, based on the scalp EEG signals, after constructing the functional networks, the subsequent statistics cannot always report the variabilities across participants, due to multiple irrelevant factors. As a

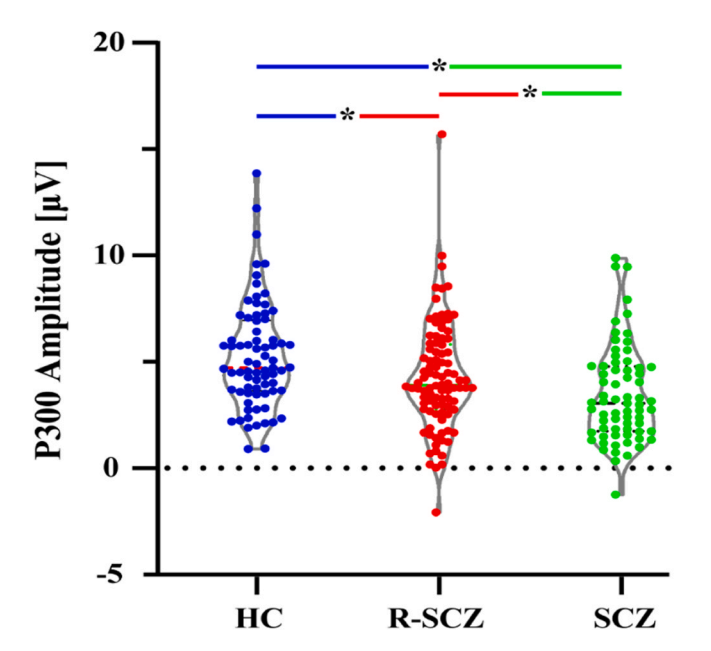


**Fig. 3.** Statistics in P300 amplitudes among the three groups. The blue-, red-, and green-colored violins denote the HC, R-SCZ, and SCZ, respectively, and the binary color-coded line with an asterisk reflects the significant difference in P300 amplitudes between the two groups under a significance level of 0.05.

**Table 2** Classification performances based on the P300 amplitude and reconstructed resting-state networks.

	P300 amplitudes	Network properties	Network topologies
Accuracy	$38.86\% \pm 9.31\%$	$39.67\% \pm 8.01\%$	$94.93\% \pm 4.82\%$
Precision	$20.76\% \pm 13.03\%$	$13.22\% \pm 2.67\%$	$95.28\% \pm 8.05\%$
Recall	$36.65\% \pm 4.06\%$	$33.33\% \pm 0.01\%$	$93.81\% \pm 11.24\%$
F1-score	$23.87\% \pm 10.08\%$	$18.79\% \pm 2.61\%$	$93.88\% \pm 6.57\%$

consequence, those latent disease-specific variations were hidden. Hence, in our current study, we newly iterated the framework of cVAEs applied in the contrasts among three groups, aiming to disentangle both patient- and relative-specific variations from the shared background across groups. Primarily, the statistical comparison between the reconstructed and original resting-state networks in Fig. 1 validated the validity of this new framework of cVAEs applied in the three groups. Hence, we accordingly acquired the latent patient- and relative-specific variations and then reconstructed their resting-state networks.

The information transition and processing in the brain largely rely on efficient network configurations. For SCZ, previous studies have widely reported disconnected communications among multiple brain regions, including frontal lobes (Ohtani et al., 2014; Ranlund et al., 2016). Herein, based on the reconstructed networks, we explored potential network distortions among the three groups, which revealed decreased inner-frontal connectivity and increased frontal-occipital connectivity in both SCZ and R-SCZ. As demonstrated previously (Broyd et al., 2009; Ongur et al., 2010), SCZ patients were found to show increased sensitivity to both the external environment and self-referential or introspective thought, thus leading to stronger activity represented by the resting-state long-range connectivity. In the meantime, frontal hypoconnectivity is also widely reported (Di Lorenzo et al., 2015) and is independent of the duration of the SCZ course. The impairment in resting-state frontal connectivity is thus believed to be one of the measures of long-lasting cognitive deficit in SCZ. Given both SCZ and their relatives carry similar pathogenic genes, herein, when compared to HC, abnormal topological patterns were identified in both SCZ and R-SCZ, which illustrated that their shared abnormalities are considered to be the genetically driven markers of risk (Sullivan et al., 2003). Furthermore, when specifically exploring the networks of SCZ and R-SCZ, the differences in Fig. 2 further validated this tendency, as stronger long-rang frontal-parietal connectivity was also uncovered for SCZ.

However, when further investigating the difference in resting-state network properties, no differences were found for both original and reconstructed networks. Considering these network properties were mainly the direct statistical measurements of the networks, although essentially derived from the networks, they still cannot encompass the entire information hidden in network topologies. And when using these network properties to classify the three groups (HC vs. SCZ vs. R-SCZ), we only acquired the unsatisfying accuracy of 31.56%  $\pm$  7.51% for the original networks and 34.75%  $\pm$  6.30% for the reconstructed networks. By contrast, the network topologies describe more details of the allocation of relevant brain resources, particularly outlining the hubs in the configuration (Li et al., 2023; Xu et al., 2014a). In fact, in our previous studies, we have already clarified the lower accuracy acquired by adopting network properties as the discriminative features than that of network topologies (Li et al., 2019). In essence, apart from providing plenty of accounts for elaborating the illness-induced distortions (Fox and Raichle, 2007), the network topologies had been widely applied in the recognition of different variables (Gomez-Pilar et al., 2016). Herein, by adopting the F-score to screen the salient features of the network topologies, we acquired the highest accuracy of 96.80%  $\pm$  2.87%, along with the precision of 95.05%  $\pm$  4.28%, recall of 98.18%  $\pm$  3.83%, and F1-score of 96.51%  $\pm$  2.83%. These reminded us that based on the reconstructed resting-state networks, we could achieve reliable recognition of SCZ and their relatives from healthy populations.

When occupied in the requested tasks, a target stimulus can evoke a clear P300 only if the related information is efficiently processed in the brain (Bledowski et al., 2004; Musso et al., 2011). Whereas, the dysfunctional brain would then lead to P300 deficits, including decreased amplitude and prolonged latency (Daffner et al., 2003). In essence, P300 has been widely accepted as an endophenotype of SCZ, herein, after matching participants who had both resting-state and task designs, the comparison in P300 amplitudes was first performed. And as displayed in Fig. 3, we did find decreased P300 amplitudes in both SCZ and R-SCZ when compared to that of HC, implying the P300 amplitudes could be used in the classification of the three groups. However, it was unexpected that when using the P300 amplitudes as the discriminative features, we only acquired an accuracy of 38.86%  $\pm$  9.31%, which was clearly lower than expected. On the contrary, the classification based on the reconstructed network topologies consistently achieved the highest accuracy of 94.93%  $\pm$  4.82%, which validated the validity of our proposed strategy again.

In the end, future potential works are further expected herein. In essence, growing evidence has widely reported the etiologic overlap among SCZ, schizoaffective disorder, and bipolar disorder, which makes them increasingly difficult to recognize (Laursen et al., 2009; Maier et al., 2006). Given that our current study demonstrated the superiority of this new framework of cVAEs in capturing disease-specific variations, it is thus believed to greatly help explore the pathological mechanism subserving varying mental illnesses, which would be putative electrophysiological biomarkers for clinical screening of these patients, leading to the promoted diagnosis of related mental diseases. Therefore, in our future works, those diseases which have etiologic overlaps would be investigated to validate the capacity of this newly iterated framework of cVAEs in disentangling the disease-specific variations from the shared background across groups, as well as achieve the accurate recognition of varying mental diseases.

## 4. Conclusion

Overall, by newly developing and applying the framework of cVAEs in the contrasts among the three groups, the latent network patterns corresponding to the SCZ and R-SCZ were effectively captured, based on

the reconstructed resting-state networks. And further statistics of the reconstructed resting-state networks reported the network distortions, e. g., the inner-frontal hypoconnectivity and frontal-occipital hyperconnectivity, while analyses on original networks revealed no differences. And only when the classification was accomplished based on the reconstructed network metrics, the satisfying classification performance would be acquired, as the highest accuracy of  $96.80\% \pm 2.87\%$ , along with the precision of  $95.05\% \pm 4.28\%$ , recall of  $98.18\% \pm 3.83\%$ , and F1-score of  $96.51\% \pm 2.83\%$ , was obtained. The findings of our current study consistently validated the validity of the newly iterated framework of cVAEs in three groups, and the identified network distortions will provide more evidence explaining the brain deficits in SCZ, as well as facilitate the diagnosis of SCZ from healthy populations.

#### 5. Materials and methods

### 5.1. Participants

The current research was approved by the Institutional Research Ethics Board of each participating site, which included five Bipolar-Schizophrenia Network on Intermediate Phenotypes (B-SNIP) consortium sites and three Psychosis and Affective Research Domains and Intermediate Phenotypes (PARDIP) sites. The written informed consent was accordingly collected from all participants. Herein, we mainly concentrated on three participant groups, including SCZ (N = 110, 34 females, aged  $31.88 \pm 11.50$  years), R-SCZ (N = 109, 71 females, aged  $42.99 \pm 15.27$  years), and demographically comparable HC (N = 118, 66 females, aged  $38.11 \pm 12.03$  years). The details of participants' demographic characteristics and clinical states can be found previously (Parker et al., 2021).

#### 5.2. EEG data acquisition

The resting-state and task EEG datasets were recorded by using Neuroscan Acquire and Synamps2 recording systems (Compumedrics Neuroscan, El Paso, TX). During recording, 64 Ag/AgCl electrodes were distributed following the standard 10–10 EEG system plus mastoids and CP1/2 locations to provide sampling lower on the back of the head, with nose reference and forehead ground. To guarantee the signal quality, the impedance per electrode was kept below 5  $k\Omega$ , along with the sampling rate of 1000 Hz.

On one hand, concerning the resting-state design, participants were first requested to sit relaxed, refrain from movements, and avoid excessive blinking, along with their resting-state EEG being recorded. On the other hand, as for task design, the auditory oddball task, consisting of 100 target tones (1500 Hz) and 567 standard tones (1000 Hz) delivered in a pseudorandom order at 70 dB, was performed. As depicted previously (Parker et al., 2021), once aware of the target tones, participants were requested to press a button. And during tasks, the task EEG was simultaneously collected.

### 5.3. EEG data analysis

## 5.3.1. Resting-state EEG preprocessing

To acquire reliable EEG segments for subsequent analyses, after data recording, the raw resting-state EEG data were exported into MATLAB (v2014a; MathWorks, Inc., USA). And multiple preprocessing procedures were performed to accomplish the data preprocessing, which included a neutral reference of the Reference Electrode Standardization Technique (REST) (Dong et al., 2017), [0.5, 45] Hz offline bandpass filtering, 2-s-length data segmentation, and artifact segment removal (  $\pm$  75  $\mu V$  as the threshold).

## 5.3.2. Task P300 amplitude

Concerning the task data, we mainly extracted the P300 amplitudes for all participants. Concretely, the raw task data were also first rereferenced to REST. And then, [0.5, 45] Hz bandpass filtering, [- 200, 800] ms data segmentation (0 ms indicates the stimulus onset), [- 200, 0] ms baseline correction, and artifact removal ( $\pm$ 75  $\mu V$  as the threshold) were accordingly applied to the re-referenced data, to extract the artifact-free trials. Thereafter, all of the artifact-free target trials were averaged to achieve the trial-averaged ERP for each participant. And on the electrode Pz, within a time interval of [300,600] ms after the target stimuli, P300 amplitude was extracted for each participant by averaging amplitudes within a time window of  $\pm$  20 ms centered at the largest positive peak.

### 5.3.3. Original network construction

As illustrated in previous studies (Miljevic et al., 2022), the scalp electrodes nearby usually obtain a similar contribution from cortical sources and capture a similar activity. Hence, to reduce the effect of volume conduction on further analyses, 32 sparse electrodes were picked out for the subsequent functional network analysis. Herein, the phase locking value (PLV) was applied to construct the original resting-state EEG networks. As defined, the Hilbert transform (HT) is calculated to form the analytical signal H(t) for both signals as,

$$\begin{cases} H_x(t) = x(t) + iHT_x(t) \\ H_y(t) = y(t) + iHT_y(t) \end{cases}$$
 (1)

where  $HT_x(t)$  and  $HT_y(t)$  are the HT of x(t) and y(t), t denotes a time point in x(t) and y(t), which are defined as follows:

$$\begin{cases} HT_x(t) = \frac{1}{\pi} P.V. \int_{-\infty}^{\infty} \frac{x(t')}{t - t'} dt' \\ HT_y(t) = \frac{1}{\pi} P.V. \int_{-\infty}^{\infty} \frac{y(t')}{t - t'} dt' \end{cases}$$
(2)

where the P.V. denotes the Cauchy principal value.

Thereafter, the analytical signal phases of x(t) and y(t) can be computed as,

$$\begin{cases} \phi_x = \arctan \frac{HT_x(t)}{x(t)} \\ \phi_y = \arctan \frac{HT_y(t)}{y(t)} \end{cases}$$
 (3)

Finally, the PLV is formulated as follows:

$$w^{phv} = \left| \frac{1}{N} \sum_{j=0}^{N-1} e^{i\left(\phi_x(j\Delta t) - \phi_y(j\Delta t)\right)} \right| \tag{4}$$

where  $w^{plv}$  is the connection weight,  $\phi_X(t)$  and  $\phi_Y(t)$  are the instantaneous phases of x(t) and y(t), respectively,  $\Delta t$  is the sampling period, and N denotes the sample number.

## 5.3.4. Reconstruction of resting-state network based on cVAEs

As inspired by previous reports (Aglinskas et al., 2022), the disease-specific variabilities are usually hidden in the original resting-state networks, hence, a new framework of cVAEs was accordingly iterated to extract disease-specific network architectures. In detail, relying on prior knowledge, the logical relationship between the information contained in the three groups was primarily determined; first, we set the data of the HC as the background, and the data of both SCZ and R-SCZ as the targets. We then used three probabilistic encoders, i.e.,  $q_{\phi_z}(z|x), q_{\phi_f}(f|x)$ , and  $q_{\phi_s}(s|x)$ , to estimate the posterior distribution z, f, sof the latent variables of the three sets. Besides, a decoder  $f_{\theta}(\cdot)$  was designed to reconstruct the input data by concatenating the latent variables. For both SCZ and R-SCZ, let the data pass through three encoders to obtain latent variables z, f, s, and then concatenate them to get [z, f, s], and the input data would be then reconstructed by the decoder  $f_{\theta}(\cdot)$ . For HC, only an encoder  $q_{\phi_z}(z|x)$  was used to get the latent variable of z, while f, and s were set as 0, which was concatenated to be [z, 0, 0], and we would then reconstruct the resting-state networks of HC through the decoder  $f_{\theta}(\cdot)$ . The detailed framework for the iterated cVAEs was depicted in Fig. 4 below.

For resting-state networks of both SCZ and R-SCZ, we have the following likelihood lower bounds,

$$\mathcal{L}_{x}(\mathbf{x}_{i}) = \mathbb{E}_{q_{\phi_{z}}(z)q_{\phi_{f}}(f)q_{\phi_{s}}(s)}[f_{\theta}(\mathbf{x}_{i}|\mathbf{z},f,s)] \\
-KL\left(q_{\phi_{z}}(\mathbf{z}|\mathbf{x}_{i}) \parallel p_{x}(\mathbf{z})\right) \\
-KL\left(q_{\phi_{f}}(f|\mathbf{x}_{i}) \parallel p_{x}(f)\right) \\
-KL\left(q_{\phi_{x}}(s|\mathbf{x}_{i}) \parallel p_{x}(s)\right), \tag{5}$$

where  $p_x(z)$ ,  $p_x(f)$ , and  $p_x(s)$  represent the prior distribution of the two background variables and significant variables of the latent spaces of the SCZ and R-SCZ, respectively. Here, we assume that the three prior distributions are multivariate isotropic Gaussian distributions  $p_x(z)$ ,  $p_x(f)$ ,  $p_x(s) \sim \mathcal{N}(0,I)$ .

For HC, we also have

$$\mathscr{L}_{\boldsymbol{b}}(\boldsymbol{b}_{j}) = \mathbb{E}_{q_{\boldsymbol{\phi}_{z}}(\boldsymbol{z})}[f_{\boldsymbol{\theta}}(\boldsymbol{b}_{i}|\boldsymbol{z},\boldsymbol{\theta},\boldsymbol{\theta})] - KL(q_{\boldsymbol{\phi}_{z}}(\boldsymbol{z}|\boldsymbol{b}_{i}) \parallel p_{\boldsymbol{b}}(\boldsymbol{z}))$$
(6)

where  $p_b(z)$  is the prior distribution of the latent variables of the HC, and the same assumption is also Gaussian distribution,  $p_b(z) \sim \mathcal{N}(0, I)$ .

Now, we infer z,f, s from the input data by training three encoders, i. e.,  $q_{\phi_z}, q_{\phi_f}$ , and  $q_{\phi_z}$ , respectively, to achieve feature extraction. A shared decoder  $f_{\theta}(\cdot)$  is then trained to take as input the connections of the latent variables and reconstruct the data. The Kullback-Leibler divergence between the latent space variable and the Gaussian distribution and the reconstruction error of the three sets of data are used as the loss function to train the entire model until the parameters  $\phi_z, \ \phi_f, \ \phi_s$ , and  $\theta$  are learned.

After the model training is completed, for the SCZ, we only used the encoder  $q_{\phi_s}$  to extract features and obtain s and then made z and f to be 0, concatenating z, f, s into [0,0,s] and sending it to the decoder  $f_{\theta}(\cdot)$  to get the SCZ-specific pattern. Similarly, for R-SCZ, we only used the encoder

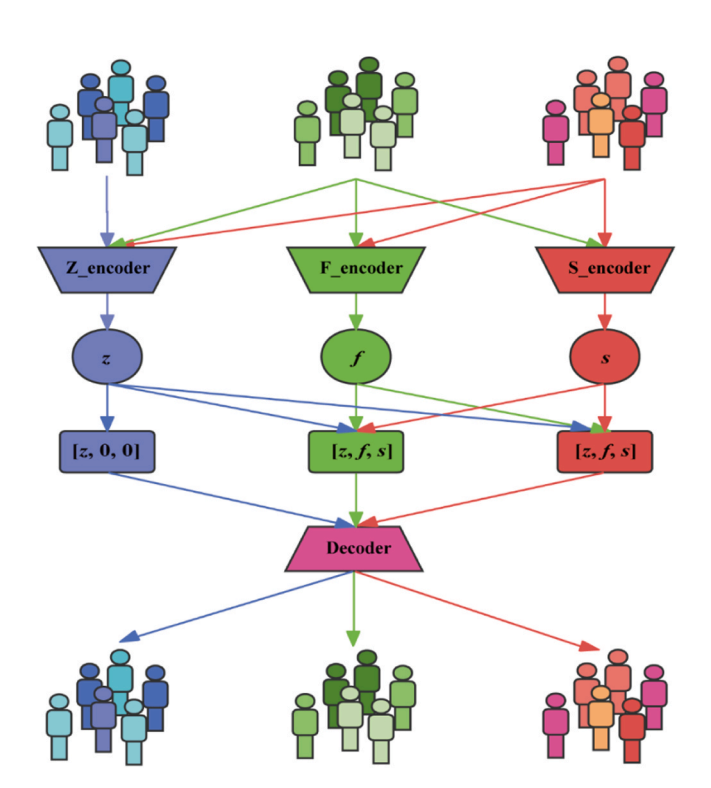


Fig. 4. The iterated framework of cVAEs applied in the contrast and reconstruction of resting-state networks among the three groups.

 $q_{\phi_f}$  and got f, let z and s be 0 and concatenate z, f, s into [0, f, 0], and using the decoder  $f_{\theta}(\cdot)$ , we would acquire the unique pattern of R-SCZ. Concerning the HC, the data would only be used as the background data by the encoder  $q_{\phi_*}$ , which is the shared mode of the three sets.

After successfully reconstructing the resting-state networks for participants in the three groups, we then statistically explored the differences in the reconstructed networks by using the independent sample *t*-tests (HC vs. SCZ, HC vs. R-SCZ, and SCZ vs. R-SCZ). And Bonferroni correction for multiple comparisons was performed to control for type I error

### 5.3.5. Resting-state network properties

Herein, to quantify the brain efficiency, two traditional network properties (i.e., CC, CPL, GE, and LE) were calculated for the reconstructed networks, by using the brain connectivity toolbox (BCT, http://www.nitrc.org/projects/bct/) (Rubinov and Sporns, 2010). In formulations, let  $w_{ij}^{pl}$  is the edge weight of the reconstructed networks between nodes i-th and j-th,  $d_{ij}$  represents the shortest weighted path length between nodes i-th and j-th, n represents the node number, and  $\Psi$  represents the set of all nodes in a given network. Both CC and CPL were then formulated as,

$$CC = \frac{1}{n} \sum_{i \in \Psi} \frac{\sum_{j,h \in \Psi} \left( w_{ij}^{plv} w_{ih}^{plv} w_{jh}^{plv} \right)^{1/3}}{\sum_{j \in \Psi} w_{ij}^{plv} \left( \sum_{j \in \Psi} w_{ij}^{plv} - 1 \right)}$$
(7)

$$CPL = \frac{1}{n} \sum_{i \in \Psi} \sum_{j \in \Psi} \frac{d_{ij}}{n - 1}$$
(8)

$$GE = \frac{1}{n} \sum_{i \in \Psi} \frac{\sum_{j \in \Psi, j \neq i} \frac{1}{d_{ij}}}{n - 1} \tag{9}$$

$$LE = \frac{1}{n} \sum_{i \in \Psi} \frac{\sum_{j,h \in \Psi, j \neq i} \left( w_{ij}^{plv} w_{ih}^{plv} \left[ d_{jh}(\Psi_i) \right]^{-1} \right)^{1/3}}{\sum_{j \in \Psi} w_{ij}^{plv} \left( \sum_{j \in \Psi} w_{ij}^{plv} - 1 \right)}$$
(10)

## 5.3.6. Classification among the three groups

It is clinically illustrated that both SCZ and R-SCZ consistently carry disease-specific genes, thus, accurately recognizing both from healthy populations always draws huge attention. Herein, we eventually tried if the captured electrophysiological metrics could be applied to facilitate the classification of the three groups. Thus, both resting-state network properties and topologies were accordingly extracted and regarded as the discriminative features, and the Support Vector Machine (SVM) classifier with a 10-fold cross-validation strategy was used to achieve the classification. Furthermore, the classification performance of restingstate networks would be also confirmed by comparing with the accuracies of using the P300 amplitude. Of note, taking the reconstructed resting-state network topologies as examples, during each time of crossvalidation, all participants were assigned to the independent testing and training set; and during the training process, to avoid overfitting, by adopting the F-score, distinguished edges with the 5% largest F-score value were extracted, along with their connectivity strengths being regarded as the discriminative features to train the SVM classifier. Thereafter, the testing features were extracted from the testing set following the rules formed in the training set, which would be further inputted into the trained SVM classifier to acquire the classification results. To avoid randomization, these procedures were repeated 1000 times, along with the average accuracy, precision, recall, and F1-score being reported. The detailed formulations of these indices were depicted as follows,

$$Accuracy = \frac{TP + TN}{TP + RP + TN + FN} \times 100\%$$
 (11)

$$Recall = \frac{TP}{TP + FN} \times 100\% \tag{12}$$

$$Precision = \frac{TP}{TP + FP} \times 100\% \tag{13}$$

$$F_1 - score = 2 * \frac{Precision * Recall}{Precision + Recall} \times 100\%$$
 (14)

where *TP* indicates the positive group of being correctly predicted, *TN* indicates the negative group of being correctly predicted, *FP* indicates the positive group of being wrongly predicted, and *FN* indicates the negative group of being wrongly predicted.

#### **Funding**

This work was supported by the China Postdoctoral Science Foundation (2021M700701), the National Natural Science Foundation of China (#62103085, #U19A2082), the STI 2030-Major Projects (#2022ZD0211400, #2022ZD0208500, #2022ZD0208900), the Key R&D projects of Science & Technology Department of Sichuan Province (#23ZDYF0961), and the Scientific Research Foundation of Sichuan Provincial People's Hospital (#2021LY21).

#### CRediT authorship contribution statement

Conceptualization: F.L. and P.X.; Data curation: D.D.; Formal analysis: F.L., G.W., and L.J.; Funding acquisition: F.L. and P.X.; Methodology: F.L. and G.W.; Supervision: D.Y., P.X., and B.H.; Validation: L.J.; Roles/Writing - original draft: F.L. G.W., and D.D.; Writing - review & editing: D.Y., X.M., and B.H.

## **Declaration of Competing Interest**

None.

#### **Data Availability**

The dataset is a publicly available dataset with a detailed description provided in Materials and Methods.

## References

- Aglinskas, A., Hartshorne, J.K., Anzellotti, S., 2022. Contrastive machine learning reveals the structure of neuroanatomical variation within autism. Science 376 (6597), 1070. https://doi.org/10.1126/science.abm2461.
- Ahangari, M., Gentry, A.E., Irish Schizophrenia Genomics, C., Nguyen, T.H., Kirkpatrick, R., Verrelli, B.C., Bacanu, S.A., Kendler, K.S., Webb, B.T., Riley, B.P., 2022. Evaluating the role of common risk variation in the recurrence risk of schizophrenia in multiplex schizophrenia families. Transl. Psychiatry 12 (1), 291. https://doi.org/10.1038/s41398-022-02060-3.
- Bassett, D.S., Sporns, O., 2017. Network neuroscience. Nat. Neurosci. 20 (3), 353–364. https://doi.org/10.1038/nn.4502.
- Bledowski, C., Prvulovic, D., Hoechstetter, K., Scherg, M., Wibral, M., Goebel, R., Linden, D.E., 2004. Localizing P300 generators in visual target and distractor processing: a combined event-related potential and functional magnetic resonance imaging study. J. Neurosci.: Off. J. Soc. Neurosci. 24 (42), 9353–9360. https://doi. org/10.1523/JNEUROSCI.1897-04.2004.
- Broyd, S.J., Demanuele, C., Debener, S., Helps, S.K., James, C.J., Sonuga-Barke, E.J., 2009. Default-mode brain dysfunction in mental disorders: a systematic review. Neurosci. Biobehav. Rev. 33 (3), 279–296. https://doi.org/10.1016/j. neubjorev.2008.09.002.
- Choi, S., Kim, M., Park, H., Kim, T., Moon, S.Y., Lho, S.K., Lee, J., Kwon, J.S., 2022. Volume deficits in hippocampal subfields in unaffected relatives of schizophrenia patients with high genetic loading but without any psychiatric symptoms. Schizophr. Res 240, 125–131. https://doi.org/10.1016/j.schres.2021.12.037.
  Chun, J., Karam, Z.N., Marzinzik, F., Kamali, M., O'Donnell, L., Tso, I.F., Manschreck, T.
- Chun, J., Karam, Z.N., Marzınzık, F., Kamalı, M., O'Donnell, L., Tso, I.F., Manschreck, T. C., McInnis, M., Deldin, P.J., 2013. Can P300 distinguish among schizophrenia, schizoaffective and bipolar I disorders? An ERP study of response inhibition. Schizophr. Res 151 (1–3), 175–184. https://doi.org/10.1016/j.schres.2013.10.020.

- da Cruz, J.R., Favrod, O., Roinishvili, M., Chkonia, E., Brand, A., Mohr, C., Figueiredo, P., Herzog, M.H., 2020. EEG microstates are a candidate endophenotype for schizophrenia. Nat. Commun. 11 (1) https://doi.org/10.1038/s41467-020-16914-1.
- Daffner, K., Scinto, L., Weitzman, A., Faust, R., Rentz, D., Budson, A., Holcomb, P., 2003. Frontal and parietal components of a cerebral network mediating voluntary attention to novel events. J. Cogn. Neurosci. 15 (2), 294–313. https://doi.org/ 10.1162/089892903321208213.
- Di Lorenzo, G., Daverio, A., Ferrentino, F., Santarnecchi, E., Ciabattini, F., Monaco, L., Lisi, G., Barone, Y., Di Lorenzo, C., Niolu, C., et al., 2015. Altered resting-state EEG source functional connectivity in schizophrenia: the effect of illness duration. Front Hum. Neurosci. 9 https://doi.org/10.3389/fnhum.2015.00234.
- Dong, L., Li, F., Liu, Q., Wen, X., Lai, Y., Xu, P., Yao, D., 2017. MATLAB toolboxes for reference electrode standardization technique (REST) of scalp EEG. Front Neurosci. 11, 601 https://doi.org/10.3389/fnins.2017.00601.
- Feng, Y., Kang, X., Wang, H., Cong, J., Zhuang, W., Xue, K., Li, F., Yao, D., Xu, P., Zhang, T., 2023. The relationships between dynamic resting-state networks and social behavior in autism spectrum disorder revealed by fuzzy entropy-based temporal variability analysis of large-scale network. Cereb. cortex 33 (3), 764–776. https://doi.org/10.1093/cercor/bhac100.
- Fox, M.D., Raichle, M.E., 2007. Spontaneous fluctuations in brain activity observed with functional magnetic resonance imaging. Nat. Rev. Neurosci. 8 (9), 700–711. https:// doi.org/10.1038/nrn2201.
- Gomez-Pilar, J., Poza, J., Bachiller, A., Nunez, P., Gomez, C., Lubeiro, A., Molina, V., Hornero, R., 2016. Novel Measure of the Weigh Distribution Balance on the Brain Network: Graph Complexity Applied to Schizophrenia. Conf Proc. IEEE Eng Med Biol Soc, pp. 700–703.
- Insel, T.R., 2010. Rethinking schizophrenia. Nature 468 (7321), 187–193. https://doi.org/10.1038/nature09552.
- Jeon, Y.W., Polich, J., 2003. Meta-analysis of P300 and schizophrenia: Patients, paradigms, and practical implications. Psychophysiology 40 (5), 684–701. https://doi.org/10.1111/1469-8986.00070.
- Jiang, L., Wang, J., Dai, J., Li, F., Chen, B., He, R., Liao, Y., Yao, D., Dong, W., Xu, P., 2022. Altered temporal variability in brain functional connectivity identified by fuzzy entropy underlines schizophrenia deficits. J. Psychiatr. Res 148, 315–324. https://doi.org/10.1016/j.jpsychires.2022.02.011.
- Jiang, L., Peng, Y., He, R., Yang, Q., Yi, C., Li, Y., Zhu, B., Si, Y., Zhang, T., Biswal, B.B., et al., 2023a. Transcriptomic and macroscopic architectures of multimodal covariance network reveal molecular-structural-functional co-alterations. Research 6, 0171. https://doi.org/10.34133/research.0171.
- Jiang, L., Yang, Q., He, R., Wang, G., Yi, C., Si, Y., Yao, D., Xu, P., Yu, L., Li, F., 2023b. Edge-centric functional network predicts risk propensity in economic decision-making: evidence from a resting-state fMRI study. Cereb. cortex. https://doi.org/ 10.1093/cercor/bhad169.
- Laursen, T.M., Agerbo, E., Pedersen, C.B., 2009. Bipolar disorder, schizoaffective disorder, and schizophrenia overlap: a new comorbidity index. J. Clin. Psychiatry 70 (10), 1432–1438. https://doi.org/10.4088/JCP.08m04807.
- Lepock, J.R., Mizrahi, R., Korostil, M., Bagby, R.M., Pang, E.W., Kiang, M., 2018. Event-related potentials in the clinical high-risk (CHR) state for psychosis: a systematic review. Clin. EEG Neurosci. 49 (4), 215–225. https://doi.org/10.1177/1550059418755212.
- Li, C., Li, P., Zhang, Y., Li, N., Si, Y., Li, F., Cao, Z., Chen, H., Chen, B., Yao, D., et al., 2023. Effective emotion recognition by learning discriminative graph topologies in EEG Brain networks. IEEE Trans. Neural Netw. Learn Syst. 1. https://doi.org/ 10.1109/fmls.2023.3238519.
- Li, F., Wang, J., Jiang, Y., Si, Y., Peng, W., Song, L., Jiang, Y., Zhang, Y., Dong, W., Yao, D., et al., 2018. Top-down disconnectivity in schizophrenia during P300 tasks. Front Comput. Neurosci. 12, 33 https://doi.org/10.3389/fncom.2018.00033.
- Li, F., Wang, J., Liao, Y., Yi, C., Jiang, Y., Si, Y., Peng, W., Yao, D., Zhang, Y., Dong, W., et al., 2019. Differentiation of schizophrenia by combining the spatial EEG brain network patterns of rest and task P300. IEEE Trans. Neural Syst. Rehabil. Eng.: a Publ. IEEE Eng. Med. Biol. Soc. 27 (4), 594–602. https://doi.org/10.1109/tnsre.2019.2900725
- Li, F., Jiang, L., Liao, Y., Li, C., Zhang, Q., Zhang, S., Zhang, Y., Kang, L., Li, R., Yao, D., et al., 2022. Recognition of the multi-class schizophrenia based on the resting-state EEG network topology. Brain Topogr. 35, 495–506. https://doi.org/10.1007/s10548-022-00907-y.
- Maier, W., Zobel, A., Wagner, M., 2006. Schizophrenia and bipolar disorder: differences and overlaps. Curr. Opin. Psychiatr. 19 (2).
- Miljevic, A., Bailey, N.W., Vila-Rodriguez, F., Herring, S.E., Fitzgerald, P.B., 2022. Electroencephalographic connectivity: a fundamental guide and checklist for optimal study design and evaluation. Biol. Psychiat-Cogn. N. 7 (6), 546–554. https:// doi.org/10.1016/j.bpsc.2021.10.017.
- Mouchlianitis, E., Bloomfield, M.A., Law, V., Beck, K., Selvaraj, S., Rasquinha, N., Waldman, A., Turkheimer, F.E., Egerton, A., Stone, J., 2015. Treatment-resistant schizophrenia patients show elevated anterior cingulate cortex glutamate compared to treatment-responsive. Schizophr. Bull. 744–752. https://doi.org/10.1093/schbul/sbv151.
- Murillo-Garcia, N., Diaz-Pons, A., Fernandez-Cacho, L.M., Miguel-Corredera, M., Martinez-Barrio, S., Ortiz-Garcia de la Foz, V., Neergaard, K., Ayesa-Arriola, R., 2022. A family study on first episode of psychosis patients: exploring neuropsychological performance as an endophenotype. Acta Psychiatr. Scand. 145 (4), 384–396. https://doi.org/10.1111/acps.13404.
- Musso, F., Brinkmeyer, J., Ecker, D., London, M.K., Thieme, G., Warbrick, T., Wittsack, H.J., Saleh, A., Greb, W., de Boer, P., et al., 2011. Ketamine effects on brain function-simultaneous fMRI/EEG during a visual oddball task. NeuroImage 58 (2), 508–525. https://doi.org/10.1016/j.neuroimage.2011.06.045.

- Nunez, P., Poza, J., Bachiller, A., Gomez-Pilar, J., Lubeiro, A., Molina, V., Hornero, R., 2017. Exploring non-stationarity patterns in schizophrenia: neural reorganization abnormalities in the alpha band. J. Neural Eng. 14 (4), 046001 https://doi.org/ 10.1088/1741-2552/aa6e05.
- Ohtani, T., Bouix, S., Hosokawa, T., Saito, Y., Eckbo, R., Ballinger, T., Rausch, A., Melonakos, E., Kubicki, M., 2014. Abnormalities in white matter connections between orbitofrontal cortex and anterior cingulate cortex and their associations with negative symptoms in schizophrenia: a DTI study. Schizophr. Res 157 (1), 190–197. https://doi.org/10.1016/j.schres.2014.05.016.
- Ongur, D., Lundy, M., Greenhouse, I., Shinn, A.K., Menon, V., Cohen, B.M., Renshaw, P. F., 2010. Default mode network abnormalities in bipolar disorder and schizophrenia. Psychiatry Res 183 (1), 59–68. https://doi.org/10.1016/j.pscychresns.2010.04.008.
- Parker, D.A., Trotti, R.L., McDowell, J.E., Keedy, S.K., Hill, S.K., Gershon, E.S., Ivleva, E. I., Pearlson, G.D., Keshavan, M.S., Tamminga, C.A., et al., 2021. Auditory oddball responses across the schizophrenia-bipolar spectrum and their relationship to cognitive and clinical features. Am. J. Psychiat 178 (10), 952–964. https://doi.org/10.1176/appi.ajp.2021.20071043.
- Raichle, M.E., 2010. The Brain's Dark Energy. Sci. Am. 302 (3), 44–49. https://doi.org/ 10.1038/scientificamerican0310-44.
- Ranlund, S., Adams, R.A., Diez, A., Constante, M., Dutt, A., Hall, M.H., Maestro Carbayo, A., McDonald, C., Petrella, S., Schulze, K., et al., 2016. Impaired prefrontal synaptic gain in people with psychosis and their relatives during the mismatch negativity. Hum. brain Mapp. 37 (1), 351–365. https://doi.org/10.1002/ hbm.23035.
- Rubinov, M., Sporns, O., 2010. Complex network measures of brain connectivity: uses and interpretations. NeuroImage 52 (3), 1059–1069. https://doi.org/10.1016/j. neuroimage.2009.10.003.
- Si, Y., Jiang, L., Li, P., Chen, B., Wan, F., Yu, J., Yao, D., Li, F., Xu, P., 2023. Relationship between decision-making and resting-state EEG in adolescents with different emotional stabilities, 1-1 IEEE Trans. Cogn. Dev. Syst.. https://doi.org/10.1109/ tcds.2023.3263845.
- Sporns, O., 2022. The complex brain: connectivity, dynamics, information. Trends Cogn. Sci. 26 (12), 1066–1067. https://doi.org/10.1016/j.tics.2022.08.002.
- Stephan, K.E., Friston, K.J., Frith, C.D., 2009. Dysconnection in schizophrenia: from abnormal synaptic plasticity to failures of self-monitoring. Schizophr. Bull. 509–527. https://doi.org/10.1093/schbul/sbn176.
- Sullivan, P.F., Kendler, K.S., Neale, M.C., 2003. Schizophrenia as a complex trait Evidence from a meta-analysis of twin studies. Arch. Gen. Psychiatry 60 (12), 1187–1192. https://doi.org/10.1001/archpsyc.60.12.1187.

- Turetsky, B.I., Dress, E.M., Braff, D.L., Calkins, M.E., Green, M.F., Greenwood, T.A., Gur, R.E., Gur, R.C., Lazzeroni, L.C., Nuechterlein, K.H., 2015. The utility of P300 as a schizophrenia endophenotype and predictive biomarker: clinical and sociodemographic modulators in COGS-2. Schizophr. Res 163 (1), 53–62. https://doi.org/10.1016/j.schres.2014.09.024.
- Wang, B., Zartaloudi, E., Linden, J.F., Bramon, E., 2022. Neurophysiology in psychosis: the quest for disease biomarkers. Transl. Psychiatry 12 (1), 100. https://doi.org/ 10.1038/s41398-022-01860-x.
- Woodward, N.D., Rogers, B., Heckers, S., 2011. Functional resting-state networks are differentially affected in schizophrenia. Schizophr. Res 130 (1–3), 86–93. https:// doi.org/10.1016/j.schres.2011.03.010.
- Xu, P., Xiong, X., Xue, Q., Li, P., Zhang, R., Wang, Z., Valdes-Sosa, P.A., Wang, Y., Yao, D., 2014a. Differentiating between psychogenic nonepileptic seizures and epilepsy based on common spatial pattern of weighted EEG resting networks. IEEE Trans. bio-Med. Eng. 61 (6), 1747–1755. https://doi.org/10.1109/TBME.2014.2305159.
- Xu, P., Xiong, X., Xue, Q., Tian, Y., Peng, Y., Zhang, R., Li, P., Wang, Y., Dezhong, Y., 2014b. Recognizing mild cognitive impairment based on network connectivity analysis of resting EEG with zero reference. Physiol. Meas. 35 (7), 1279–1298. https://doi.org/10.1088/0967-3334/35/7/1279.
- Yang, A.C., Hong, C.J., Liou, Y.J., Huang, K.L., Huang, C.C., Liu, M.E., Lo, M.T., Huang, N.E., Peng, C.K., Lin, C.P., et al., 2015. Decreased resting-state brain activity complexity in schizophrenia characterized by both increased regularity and randomness. Hum. brain Mapp. 36 (6), 2174–2186. https://doi.org/10.1002/ hbm.22763.
- Yang, Y., Jiang, L., He, R., Song, P., Xu, P., Wang, Y., Li, F., 2023. Repetitive transcranial magnetic stimulation modulates long-range functional connectivity in autism spectrum disorder. J. Psychiatr. Res 160, 187–194. https://doi.org/10.1016/j. jpsychires.2023.02.021.
- Yi, C., Yao, R., Song, L., Jiang, L., Si, Y., Li, P., Li, F., Yao, D., Zhang, Y., Xu, P., 2022. A novel method for constructing EEG large-scale cortical dynamical functional network connectivity (dFNC): WTCS. IEEE Trans. Cyber 52 (12), 12869–12881. https://doi.org/10.1109/TCYB.2021.3090770.
- Zhang, T., Liu, T., Li, F., Li, M., Liu, D., Zhang, R., He, H., Li, P., Gong, J., Luo, C., et al., 2016. Structural and functional correlates of motor imagery BCI performance: Insights from the patterns of fronto-parietal attention network. NeuroImage 134, 475–485. https://doi.org/10.1016/j.neuroimage.2016.04.030.